AFRL-ML-WP-TP-2006-453

X-RAY LINE-BROADENING INVESTIGATION OF DEFORMATION DURING HOT ROLLING OF Ti-6Al-4V WITH A COLONY-ALPHA MICROSTRUCTURE (PREPRINT)

M.G. Glavicic and Sheldon L. Semiatin

JULY 2006

Approved for public release; distribution is unlimited.

STINFO COPY

This work, resulting in whole or in part from Department of the Air Force contract number F33615-04-D-5235, has been submitted to Elsevier B.V. for publication in Acta Materialia.

MATERIALS AND MANUFACTURING DIRECTORATE
AIR FORCE RESEARCH LABORATORY
AIR FORCE MATERIEL COMMAND
WRIGHT-PATTERSON AIR FORCE BASE, OH 45433-7750

REPORT DOCUMENTATION PAGE

Form Approved
OMB No. 0704-0188

1. REPORT DATE *(DD-MM-YY)*	2. REPORT TYPE	3. DATES COVERED *(From - To)*
July 2006	Journal Article Preprint	

4. TITLE AND SUBTITLE

X-RAY LINE-BROADENING INVESTIGATION OF DEFORMATION DURING HOT ROLLING OF Ti-6Al-4V WITH A COLONY-ALPHA MICROSTRUCTURE (PREPRINT)

5a. CONTRACT NUMBER
F33615-04-D-5235

5b. GRANT NUMBER

5c. PROGRAM ELEMENT NUMBER
63883C

6. AUTHOR(S)

M.G. Glavicic (UES, Inc.)
Sheldon L. Semiatin (AFRL/MLLMP)

5d. PROJECT NUMBER
9201

5e. TASK NUMBER
29

5f. WORK UNIT NUMBER
92012901

7. PERFORMING ORGANIZATION NAME(S) AND ADDRESS(ES)

UES, Inc.
4401 Dayton-Xenia Road
Dayton, OH 45432-1894

Metals Branch (AFRL/MLLMP)
Metals, Ceramics and NDE Division
Materials and Manufacturing Directorate
Air Force Research Laboratory, Air Force Materiel Command
Wright-Patterson AFB, OH 45433-7750

8. PERFORMING ORGANIZATION REPORT NUMBER

9. SPONSORING/MONITORING AGENCY NAME(S) AND ADDRESS(ES)

Materials and Manufacturing Directorate
Air Force Research Laboratory
Air Force Materiel Command
Wright-Patterson AFB, OH 45433-7750

10. SPONSORING/MONITORING AGENCY ACRONYM(S)
AFRL-ML-WP

11. SPONSORING/MONITORING AGENCY REPORT NUMBER(S)
AFRL-ML-WP-TP-2006-453

12. DISTRIBUTION/AVAILABILITY STATEMENT
Approved for public release; distribution is unlimited.

13. SUPPLEMENTARY NOTES
This work, resulting in whole or in part from Department of the Air Force contract number F33615-04-D-5235, has been submitted to Elsevier B.V. for publication in Acta Materialia.

14. ABSTRACT

X-ray line-broadening techniques that were previously developed and applied to quantify deformation behavior during the hot rolling of commercial-purity titanium were applied for Ti-6AI-4V plate with a colony-alpha preform microstructure. The present work quantified the challenges in using line-broadening techniques for two-phase titanium alloys which undergo a phase transformation during cooling following hot working.

15. SUBJECT TERMS
titanium, substructure, texture, line-broadening, strain-partitioning

16. SECURITY CLASSIFICATION OF:			17. LIMITATION OF ABSTRACT:	18. NUMBER OF PAGES	19a. NAME OF RESPONSIBLE PERSON (Monitor)
a. REPORT	b. ABSTRACT	c. THIS PAGE			Sheldon L. Semiatin
Unclassified	Unclassified	Unclassified	SAR	42	19b. TELEPHONE NUMBER *(Include Area Code)* N/A

X-Ray Line-Broadening Investigation of Deformation during Hot Rolling of Ti-6Al-4V with a Colony-Alpha Microstructure

M.G. Glavicic*, and S.L. Semiatin

Air Force Research Laboratory, Materials and Manufacturing Directorate,
AFRL/MLLMP, Wright-Patterson AFB, OH 45433-7817
*UES, Inc., 4401 Dayton-Xenia Road, Dayton, OH 45432

Abstract

X-ray line-broadening techniques that were previously developed and applied to quantify deformation behavior during the hot rolling of commercial-purity titanium were applied for Ti-6Al-4V plate with a colony-alpha preform microstructure. The present work quantified the challenges in using line-broadening techniques for two-phase titanium alloys which undergo a phase transformation during cooling following hot working.

Keywords

Titanium, substructure, texture, line-broadening, strain-partitioning

1. Introduction

An understanding of deformation behavior in terms of slip and twinning activity is required for the modeling of texture and microstructure evolution during the thermomechanical processing of metallic materials. A method to determine how the macroscopically imposed strain is partitioned is also required for two-phase alloys. The measurement of dislocation type and density in industrially-processed materials can be

very difficult using conventional techniques such as transmission-electron microscopy (TEM) because of the high strain levels encountered and thus the large number of dislocations that are introduced. In such instances, x-ray and neutron line-broadening are attractive alternative techniques to quantify substructure evolution. These methods provide statistically-averaged information over the area/volume irradiated. Furthermore, the broadening of the diffraction peaks from different phases can be analyzed to determine the slip activity within each phase of a multi-phase alloy. The main disadvantage of using x-ray and neutron line-broadening techniques, however, is that individual diffraction peaks can also be broadened by a number of other microstructural features, each of whose influence must be taken into account to obtain an accurate estimate of dislocation density. In addition, the amount of second phase in two-phase alloys may be very low (< 10%), and the material may be highly textured; both of these factors may limit the number of diffraction peaks available for analysis.

The characterization of material defects using x-ray and neutron-diffraction techniques has received considerable attention during the past few decades. Originally formulated for polycrystalline powders [1-7], such methods have been extended to examine defects in single crystals [8-11] and grain/subgrain sizes in polycrystalline materials [12,13]. They have also been used to establish the substructure in individual texture components of rolled commercial-purity titanium (CP Ti) sheet [14, 15] and to isolate the line-broadening effect of specific texture components [16, 17]. Most recently, x-ray line broadening has been applied to establish the relative activity of slip systems in deformed materials with a hexagonal-close-packed (hcp) crystal structure [13, 18, 19]. In Reference 19, for example, a specific averaging and analysis techniques was developed to

determine the relative activity of various slip systems during deformation and the overall dislocation density. Such results were also used to interpret the incidence and magnitude of twinning and dynamic recovery over a wide range of temperature.

The main objective of the present work was to extend the previous approach for unalloyed, single-phase titanium [19] to a two-phase (alpha/beta) titanium alloy, Ti-6Al-4V, with a colony-alpha preform microstructure.

2. Theoretical Background

A brief review of previous work on x-ray line-broadening (for cubic and hcp materials) and strain partitioning during the deformation of two-phase materials is presented below to illustrate the basis for the procedures and simplifications used in the present work.

2.1 Diffraction line-breadth analysis in hcp materials

The presence of dislocations in a crystal interrupts the periodicity of a lattice and causes diffraction-line broadening. The quantitative effect of randomly distributed dislocations on diffraction patterns was first studied by Krivoglaz and Ryaboshapka [1], Krivoglaz, et al. [2], and Wilkens [11, 20, 21]. More recently, Wu, et al. [22, 23] obtained the following expression to describe the integral breadth β of a diffraction peak from an ensemble of randomly oriented dislocations:

$$\beta^2 = \rho\chi f(M)\tan^2\theta, \tag{1}$$

in which ρ is the dislocation density, χ is the orientation factor, and θ is the Bragg angle of the diffraction peak. The analytical function $f(M)$ describes the relationship between M and the integral breadth of profiles, where $M=R_e\rho^{1/2}$ and R_e is the outer cutoff radius of the dislocations. In essence, $f(M)$ takes various values depending on the dislocation

distribution. An analytical expression for the function *f(M)* was also derived by Wu, et al. [22] with an accuracy of 3 pct. over the range $0.1 \leq M \leq 10$. The form of this function was:

$$f(M) = a\ln(M+1) + b\ln^2(M+1) + c\ln^3(M+1) + d\ln^4(M+1), \qquad (2)$$

in which a = -0.173, b = 7.797, c = -4.818, and d = 0.911. The general method for inferring M from a measured diffraction peak comprises the determination of the Fourier-series coefficients *A(L)* for the diffraction peak. It has been shown in reference 19 that from a plot of $ln[A(L)]/L^2$ versus *ln[L]* for low to intermediate values of L, M can then be deduced using the slope ξ and intercept ψ in which:

$$M \cong \frac{1}{3}|\xi|^{1/2} e^{-\psi/\xi}. \qquad (3)$$

For unalloyed, commercial-purity (CP) titanium, it was shown previously [19] that the integral breadths derived form the experimental data (Eq. (1)) can be analyzed using the best-fit linear plot of $\beta/\langle\chi\rangle^{1/2}$-versus-$\tan\theta$, in which $\langle\chi\rangle$ denotes an average orientation factor constructed from the orientation factors of the slip systems considered. The specific orientation factors considered in the analysis were the $<11\bar{2}0>\{0001\}$ (basal <a>), $<11\bar{2}0>\{1\bar{1}00\}$ (prism <a>), $<11\bar{2}3>\{0\bar{1}11\}$ (pyramidal <c+a>), $<11\bar{2}3>\{2\bar{1}\bar{1}2\}$ (pyramidal <c+a>), and $<11\bar{2}3>\{11\bar{2}1\}$ (pyramidal <c+a>) edge dislocations and the $<11\bar{2}0>$ and $<11\bar{2}3>$ screw dislocations. The average orientation factor $\langle\chi\rangle$ for the specific material of interest was calculated by assigning weighting factors η, ω, and φ to the edge (χ^E) and screw (χ^S) orientation factors, using the following relation:

$$\langle\chi\rangle = \delta\left(\left|\vec{b}_{<a>}\right|^2\left(\eta\chi^E_{Basal}+\omega\chi^E_{Prism}\right)+\left|\vec{b}_{<c+a>}\right|^2\varphi\chi^E_{Pyra}\right)+(1-\delta)\left(\left|\vec{b}_{<a>}\right|^2(\eta+\omega)\chi^S_{<a>}+\left|\vec{b}_{<c+a>}\right|^2\varphi\chi^S_{<c+a>}\right) \quad (4)$$

The proportion of edge to screw dislocations was partitioned with the factor δ. The weighting factors deduced to construct the average orientation factor $\langle\chi\rangle$ were then used to explain the content of the various types of dislocations present in samples rolled at various temperatures.

2.2 Diffraction line-breadth analysis in cubic materials

For cubic materials, the critical resolved shear stresses of the individual slip systems are identical. For this reason, the weighting process used to deduce the relative activity of the various slip systems described in Section 2.1, which uses the best-fit linear plot of $\beta/\langle\chi\rangle^{1/2}$-versus-$\tan\theta$, is not required. In this case, the average orientation factor is simply a weighted average of the orientation factors for screw and edge dislocations. A common method to account for anisotropy in the broadening of diffraction peaks in cubic materials is through the use of a modified Williams-Hall plot proposed by Ungár [24]. In this technique, the broadening due to dislocations is characterized by the following relationship:

$$\Delta K \cong \frac{\gamma}{D}+\left(\frac{\pi M^2 b^2}{2}\right)^{1/2}\rho^{1/2}K\overline{C}^{1/2}+O(K^2\overline{C}), \quad (5)$$

in which D is the average particle size in the specimen, γ is a constant equal to 0.9, ρ and b are the average dislocation density and the length of the Burgers vector of dislocations, respectively. Furthermore, $\Delta K = \cos\theta[\Delta(2\theta)/\lambda]$, in which $\Delta(2\theta)$ is the full-width half-maximum (FWHM) of the diffraction peak, $K = 2\sin\theta/\lambda$, and $O(K^2\overline{C})$ stands for

(6)

higher order terms in $K^2\overline{C}$. $\overline{C}$ is the average dislocation orientation/contrast factor described by:

$$\overline{C} = \overline{C}_{h00}(1 - qH^2),$$

in which $\overline{C}_{h00}$ is the average orientation factor for the *h00* reflections, $H^2 = (h^2k^2 + h^2l^2 + k^2l^2)/(h^2 + k^2 + l^2)^2$, and q is parameter depending upon the elastic constants of the crystal and edge or screw character of dislocations.

2.3 Self-consistent model for strain partitioning

A prior self-consistent model [25] was used in the present work to quantify strain-partitioning during the deformation of a two-phase alloy* and hence to rationalize the line-broadening results. The model was based on the approach developed by Hill [26] and later extended by Suquet [27] for linearly elastic solids. Hill's analysis assumed that both phases are linearly viscoplastic; i.e., they have a constitutive relation of the form:

$$\sigma_i = k_i^L \dot{\varepsilon}_i, \tag{7}$$

in which σ and $\dot{\varepsilon}$ denote the flow stress and strain rate, respectively, k^L is the "viscosity" coefficient, and the subscripts (i = 1, 2) refer to phases 1 or 2. The viscosity of the aggregate k_{sc}^L (which relates the aggregate flow stress and strain rate) is given by the following expression:

$$k_{SC}^L / k_1^L = \left(\frac{1}{6}\right)\left\{3 - 2\rho + 5(1-f)(\rho-1) + \sqrt{[3 - 2\rho + 5\,(1-f)(\rho-1)]^2 + 24\rho}\,\right\}, \tag{8}$$

in which $\rho = k_2^L/k_1^L$, and f denotes the volume fraction of phase 1.

* The self-consistent approach used here is formally valid only for two-phase materials with equiaxed constituents, and hence its application in the present work represents an approximation.

Suquet [27] extended the above analysis to the case in which both phases are power-law viscoplastic, viz.,

$$\sigma_i = k_i \dot{\varepsilon}_i^m , \tag{9}$$

and the strain-rate sensitivity exponents for both phases are equal; i.e., $m_1 = m_2 = m$. In this case, the viscosity-like parameter of the aggregate (k) is a function of the values of viscosity-like parameters for the two phases, k_1 and k_2, as well as m, ρ, and k_{sc}^L/k_1^L:

$$k/k_1 = \min_{\rho \geq 0} \left\{ \left(k_{SC}^L / k_1^L \right)^{(m+1)/2} \left[f + (1-f)\rho^{(m+1)/(m-1)} \left(k_2/k_1 \right)^{2/(1-m)} \right]^{(1-m)/2} \right\}. \tag{10}$$

In Equation (10), the expression on the right-hand side before the argument in braces denotes the minimum value for $\rho \geq 0$. In practice, the value of k_{sc}^L/k_1^L for the corresponding linearly-viscous case is unknown. Thus, the evaluation of k/k_1 involves a procedure in which trial values of ρ are guessed, k_{sc}^L/k_1^L, is determined from Equation (8), and ρ and k_{sc}^L/k_1^L are inserted into Equation (10). The value of ρ that yields the minimum value of k/k_1 is the appropriate one.

The average strain rates in the two phases are readily calculated from the values of k, k_1, k_2, and the volume fraction f of phase 1. Following Hill [28], the aggregate flow stress σ_{ov} and strain rate $\dot{\varepsilon}_{ov}$ are volume averages of the corresponding flow stresses and strain rates in the individual phases:

$$\sigma_{ov} = k\dot{\varepsilon}_{ov}^m = fk_1\dot{\varepsilon}_1^m + (1-f)k_2\dot{\varepsilon}_2^m , \tag{11}$$

$$\dot{\varepsilon}_{ov} = f\dot{\varepsilon}_1 + (1-f)\dot{\varepsilon}_2 . \tag{12}$$

Solving Equation (12) for $\dot{\varepsilon}_2$ as a function of $\dot{\varepsilon}_{ov}$ and $\dot{\varepsilon}_1$,

(13)

$$\dot{\varepsilon}_2 / \dot{\varepsilon}_{ov} = [1 - f(\dot{\varepsilon}_1 / \dot{\varepsilon}_{ov})]/(1-f),$$

and inserting this relation into Equation (11), an expression for $\dot{\varepsilon}_1 / \dot{\varepsilon}_{ov}$ is obtained:

$$k/k_1 = f\left(\dot{\varepsilon}_1/\dot{\varepsilon}_{ov}\right)^m + \left[(1-f)^{(1-m)}\left(k_2/k_1\right)\left(1 - f\left(\dot{\varepsilon}_1/\dot{\varepsilon}_{ov}\right)\right)^m\right]. \qquad (14)$$

Equation (14) cannot be solved analytically, but is readily evaluated using numerical techniques.

Having calculated the relative strain rates at a given temperature for a given ratio of the volume fraction of the two phases, the relative strain accommodated in each of the phases can then be deduced.

3. Material and Procedures

3.1 Material

Ti-6Al-4V with a normal interstitial level (Ti-6.41Al- 3.78V-0.1Fe-0.17O-0.01N-0.01C-24 ppm H) was used to develop and validate an experimental approach to determine the dislocation content in the alpha and beta phases via an x-ray line-broadening technique. The material was received as 32-mm thick hot-rolled plate. The plate was cut into 50.8-mm × 101.6-mm blanks, which were heat treated in a series of furnaces using a cycle comprising 940°C/20 minutes + 1065°C/15 minutes + 940°C/10 minutes + air cool. Each blank was then reheated to 955°C for 45 minutes and water quenched. By this means a preform microstructure consisting of colony alpha was developed

3.2 Experimental procedures

Two sets of heat-treated Ti-6Al-4V blanks that were tapered on one end (to facilitate feeding) were prepared for rolling. One set was rolled to a reduction of 10 pct. in a single pass at various temperatures followed by water quenching (Table 1) to retain the presumed quasi-random dislocation substructure formed during rolling. The other set was rolled with no reduction to simulate the evolution of the presumed quasi-random dislocation substructure and phase transformations that would occur during the water quenching of Ti-6Al-4V. Each sample was sectioned along three orthogonal surfaces at the specimen mid-plane for characterization purposes (Fig. 1). Each of the three surfaces was perpendicular to one of the principal specimen reference directions (rolling direction (RD), transverse direction (TD), normal direction (ND)). The surfaces were then metallographically prepared for x-ray measurements using Cu K_α radiation from an 18-kW rotating anode source and for microstructural characterization using a Leica Cambridge Stereoscan 360 FE scanning-electron microscope (SEM).

Diffraction patterns were collected from the three mid-plane surfaces cut from each specimen for a scanning range of $30^\circ \leq 2\theta \leq 140^\circ$. Instrument broadening of the measured x-ray lines was corrected by running an NBS Si standard using the same x-ray optics.

The textures of the rolled samples were determined from measurement of $(10\bar{1}0)$, (0002), $(10\bar{1}1)$, $(10\bar{1}2)$, and $(11\bar{2}0)$ alpha-phase pole figures and (110) and (200) beta-phase pole figures measured in the Schultz-reflection mode at the specimen mid-plane on ND specimens (Fig. 1). The measured data were analyzed using the texture-analysis software popLA (preferred orientation package from Los Alamos National Laboratory).

3.3 Line-broadening analysis procedures

The measured breadths of individual diffraction peaks of the alpha and beta phases from the three orthogonal sections of each rolled specimen were averaged in an attempt to emulate a random polycrystalline specimen. The results were then analyzed using the following methods for the individual phases in the Ti-6Al-4V alloy.

3.3.1 Alpha phase

The average integral line breadths were analyzed to establish the relative slip-system activity in the alpha phase. The contributions of the basal, prism, and pyramidal dislocations to line broadening (i.e., weighting factors η, ω, and φ in Equation (4)) were deduced assuming a mixture of 50 pct. screw and 50 pct. edge dislocations. Specifically, the proportions of the various dislocations were systematically varied using an automated optimization approach that maximized the R^2 in a $\beta_{avg}/\langle\chi\rangle^{1/2}$-versus-$\tan\theta$ plot of the data. For this purpose, the optimization program iSIGHT™ (Version 8.0), which incorporates non-linear sequential quadratic and mixed-integer optimization subroutines to select values for the weighting factors, was used to maximize the R^2. The iSIGHT™ software was coupled to Excel™-spreadsheet plots of the data and orientation factors.

With the values of η, ω, and φ so determined, the dislocation densities in the alpha-phase were estimated from the corrected $(20\bar{2}2)_\alpha$ diffraction-peak breadth on specimens whose surface was perpendicular to either the rolling direction (RD) or the transverse direction (TD). The values of M deduced from the Fourier analysis of the shape of the diffraction peaks for each temperature (Table 1) were also used in the calculation of dislocation densities.

3.3.2 Beta phase

The average full-width half-maxima (FWHM) of the diffraction peaks for the beta phase were analyzed using the *modified* Williams-Hall technique proposed by Ungár, et al. [24]. Due to the limited number of peaks available for analysis, it was not possible to experimentally deduce the relative proportions of edge and screw dislocations in the specimens using the method proposed by Schafler, et al. [29]. Hence, a mixture of 50% screw and 50% edge dislocations was assumed to determine the average orientation/contrast factors ($\overline{C}$) of the individual diffraction peaks. In order to estimate $\overline{C}$, the elastic constants C_{11} = 97.7, C_{12} = 82.7, and C_{44} = 37.5 GPa at 1000 °C, deduced via electromagnetic-acoustic resonance [30], were used. The values for $\overline{C}$ were then obtained by extrapolating the results in the tables in Reference 31 using the standard definition of elastic anisotropy, $A = 2C_{44}/(C_{11}-C_{12})$.

Due to the low volume fraction of retained beta and hence the limited number of diffraction peaks available for analysis, the average FWHM from the measurements on three orthogonal sections was used to infer the evolution of the dislocation density in the beta phase. These averages were plotted in the form of a modified Williams-Hall plot in which the higher order terms, $O(K^2\overline{C})$, were neglected. Dislocation densities were then estimated from the slope of these plots, and the values of M determined from the Fourier analysis of the diffraction peaks for each temperature (Table 1).

3.4 Strain-partitioning analysis

The self-consistent analysis (Equations (8)-(14)) was used to quantify strain partitioning between the alpha and beta phases in Ti-6Al-4V. These analyses were conducted using the same Excel™ spread-sheet approach as in Reference 25. The values of f_α, m, and k_α/k_β were also taken from this source. Specifically, the volume fractions of

the alpha and beta phases at each rolling temperature were obtained from the beta-approach curve. The rate sensitivity m for both the alpha and beta phases was taken to be 0.23; this value of m is typical for metals whose hot deformation is controlled by the glide and climb of dislocations [32, 33]. A value of $k_\alpha/k_\beta = 3$ was used over the entire temperature range investigated per the results in Reference 25.

4. Results and Discussion

The key results of this investigation consisted of estimates of the slip activity/dislocation density in the alpha and beta phases as a function of rolling temperature. The validity of these results is then discussed in the context of the substructures formed during rolling versus those developed during quenching of samples not subjected to rolling reduction.

4.1 Microstructure at rolling temperature

Because the reduction in all cases was small (i.e., ~10 pct.), the microstructure of the Ti-6Al-4V samples underwent little change during rolling. At temperatures below 925°C, at which the volume fraction of alpha was greater than 0.5, the material exhibited a well-defined colony microstructure (Fig. 2a); in this and other micrographs, alpha is the darker phase and beta/transformed beta is the lighter constituent. At higher temperatures, at which the volume fraction of alpha was less, the lamellar structure was less well defined as a result of partial dissolution and spheroidization of the alpha lamellae (Fig. 2b). In all cases, the alpha lamellae were surrounded by a matrix of untransformed beta or fine, transformed beta, the latter consisting of laths of acicular $\alpha' + \alpha''$ (martensite) formed during water quenching following rolling. The width of these laths was ~0.5 μm.

4.2 Alpha-phase slip-system activity

The weighting factors φ and ω for the average orientation factor $\langle\chi\rangle$ for the alpha-phase peaks determined from the best fit of $\beta_{avg}/\langle\chi\rangle^{1/2}$-versus-$\tan\theta$ plots for rolled samples are shown in Fig. 3; at all temperatures, the weighting factor η was essentially equal to zero. Plots of the weighting factors indicated that the main deformation mechanisms within the temperature range investigated (800 - 975°C) comprised prism <a> and pyramidal <c+a> slip. The weighting factor φ for <c+a> dislocations increased slightly with temperature suggesting a slight decrease in the relative critical resolved shear stress of the pyramidal <c+a> slip systems relative to that for the prism <a> and basal <a> slip systems.

The observed *inactivity* of basal <a> slip, relative to prism <a> slip, may be explained in the context of the relative strengths of these deformation modes at hot working temperatures and the anisotropy of slip transfer and plastic flow in titanium alloys with a colony-alpha microstructure. With regard to the former effect, extensive prior research has shown that the critical resolved shear stress (CRSS) of the prism <a> slip system is less than [34, 35, 36] or equal to [37] that of the basal <a> slip system. In particular, it was found that the best agreement between measurements and Taylor-model predictions of the flow stress and r-values for a textured Ti-6Al-4V with a colony microstructure deformed at hot-working temperatures was obtained when the CRSS for prism <a> slip was 30% less than that for basal <a> slip. As such, prism <a> slip would predominate for colonies oriented such that the Taylor factors for basal <a> or prism <a> slip are comparable. In addition, a simple Schmid analysis of the basal <a> and prism <a> slip systems for the starting alpha-phase texture of the present Ti-6Al4V material revealed that prism <a> slip would be expected to be the predominant slip mechanism.

With regard to the anisotropy of flow in titanium alloys with a colony-alpha microstructure, room-temperature single-colony compression tests on Ti-5Al-2.5Sn-0.5Fe [38] and Ti-6Al-2Sn-4Zr-2Mo-0.1Si [39] have revealed that the values of the CRSS for the three discrete <a> slip systems (be they prism or basal) are not equivalent. This anisotropy is manifest by values of CRSS which are either lower or higher depending on whether the specific <a> slip vector is parallel or not parallel, respectively, to a <111> slip direction in the corresponding beta (bcc) matrix. The relative ease of slip transfer was found to give rise to a variation in the CRSS of prism <a> systems of the order of 10% and of basal <a> systems of the order of 30%. In other words, the two 'hard' prism or basal <a> slip directions would have a flow stress 10% or 30% greater than that for the 'soft' slip direction whose CRSS is approximately equivalent to that for a single-phase alpha microstructure. Hence, if the slip anisotropy observed at ambient temperatures persists to elevated temperatures, the difference between the CRSS values of the hard prism <a> and the hard basal <a> systems may provide a substantial bias for the activation of prism <a> slip. Although the presence of one soft prism <a> and one soft basal <a> system, whose CRSSs vary by approximately 30 pct., would reduce the overall bias, the fact that there are two hard systems would lead to prism <a> slip being favored from a statistical standpoint.

4.3 Alpha-phase dislocation densities

Previous work [19] has indicated that the dislocation density in the alpha phase should be determined using a diffraction line for a specific crystallographic plane that is randomly oriented over the entire temperature range of interest. For the present Ti-6Al-4V material, the texture was such that a diffraction line which was slightly less than

random ($(20\bar{2}2)_\alpha$) had to be selected (Fig. 4). For this line, Fourier analysis of the shape at different temperatures (Table 1) showed that the average M (determined from the RD, TD and ND sections at each specific temperature) was approximately equal to one, thus indicating that the distribution of dislocations was homogeneous and quasi-regular [22] and justifies the use of equation (3) in the ensuing analysis.

Dislocation densities were estimated from the $(20\bar{2}2)_\alpha$ diffraction line for both TD and RD specimens. Inspection of the pole-figure contour levels at the TD and RD locations (Fig. 4) showed that the corresponding texture components were essentially randomly oriented for the TD specimens, but not for the RD specimens. Thus, calculations of dislocation density for the $(20\bar{2}2)_\alpha$ line from the two different samples (using Equation (1)) served to quantify the influence of texture. The calculated dislocation density as a function of rolling temperature (Fig. 5) followed the same general trend for both specimen orientations. However, the calculations revealed that the dislocation density determined from the TD specimens, whose $(20\bar{2}2)_\alpha$ planes were indeed quasi-randomly oriented, were consistently *higher* than those determined from the RD specimens at all rolling temperatures. The difference in the results obtained from the TD and RD specimens thus emphasizes the importance of diffraction-peak selection for calculating the dislocation densities in textured materials. If the selected diffraction peak is biased by texture, the inferred dislocation density will be affected in some fashion depending upon which texture component is selected and how the dislocations are spatially oriented with respect to the diffracting plane of the specimen.

A closer examination of the calculations in Figure 5 showed that the measured dislocation densities *decreased* gradually for rolling temperatures from 800°C to 900°C

even though the total deformation was the same in all cases (~10%). The observed change in the dislocation density over this temperature interval can be attributed to two effects: (1) dynamic recovery (whose magnitude increases with temperature) which would reduce the stored dislocation content per se and (2) a reduction in the strain accommodated by the alpha phase due to a decrease in its relative volume fraction with increasing rolling temperature (Fig. 6).

At temperatures of 925°C and above, at which there is substantially less alpha phase and the microstructure is partially spheroidized (Fig. 2b), the dislocation density calculated from Eq. (1) *increased* with temperature (Fig. 5). In this regime, an acicular α' phase with a hexagonal close packed structure with lattice parameters very similar to the α phase is formed in the beta matrix during water quenching following rolling. The line broadening that could have been produced by the small width (~ 0.5 μm) of these acicular α' laths is insufficient to fully account for the observed changes in the magnitude of the diffraction peak breadths that were measured. On the other hand, TEM studies of quenched Ti-6Al-4V specimens in the literature [40] have revealed that a substructure containing dislocations and stacking faults is also formed in acicular α'. Using the extinction criteria $g \cdot b = 0$, it was found that these dislocations were predominantly of an <a>-type [41]. Therefore, it may be surmised that a possible explanation for the measured increase in the dislocation density in spite of the reduction of strain accommodated by the alpha phase at temperatures of 925°C and above is a result of dislocations that are formed in the acicular α' during water quenching.

A comparison of the diffraction patterns for undeformed and rolled specimens (Figures 7 and 8, respectively) revealed an additional source of line broadening, i.e., the

formation of orthorhombic α" phase. The lattice parameters of α" (a=3.033, b=4.924 and c=4.667 Å) are such that many of the peaks in the diffraction pattern closely coincide with the locations of the α-phase peaks. As a result, doublet peaks are found at the low 2θ locations in the patterns collected for the undeformed specimens (Fig. 7). The deduced lattice parameters also fit well with those previously published for Ti-6Al-4V [42]. In addition, the α" phase is textured and thus has a different effect on the low diffraction-angle peaks from the three specimen orientations (RD, TD, ND). Calculation of the positions of all other possible diffraction peaks from the deduced lattice parameters of the orthorhombic α" phase revealed that the peak overlap apparent at low 2θ angles was not an issue for some of the higher order α and α' phase peaks. In particular, for the $(20\bar{2}2)$ diffraction peak which was used to calculate the dislocation densities shown in Figure 5, no significant peak overlap exists since the location of the two closest orthorhombic α" peaks ({014} and {041}) are midway between the (0004) and $(20\bar{2}2)$ peaks of the α and α' phases. As such, only specimens that contain significant proportions of the α' phase will be plagued by the x-ray line broadening due to the formation of dislocations with this phase. Hence, at lower deformation temperatures, at which acicular α' is not produced, the measurements will be dominated by broadening due to dislocations formed during rolling. At higher temperatures (900°C and above), the diffraction patterns have a degree of broadening associated with the formation of the α'. Therefore, the dislocation density would be expected to increase with temperature in this regime.

The effect of the phases formed during quenching on the orientation weighting factors appears to be minimal in that the values obtained did not vary substantially over the temperature range examined in spite of the peak overlap complications that arose as a result of the formation of the α' and α". This can be explained by the fact that a total of 18 diffraction peaks were collected and used for each of the three specimen orientations. Each peak breadth measured was then averaged for the three directions (RD, TD and ND) and then used to deduce the orientation weighting factors for a single rolling temperature. As a result, the formation of textured orthorhombic α" phase during quenching only had a moderate effect on specific diffraction spectra where peak overlap and texture combined to substantially change the apparent breadth. Hence, the use of 54 diffraction spectra to assign the three most appropriate orientation weighting factors for a specific rolling temperature outweighed biasing due to peak overlap. The changes in the orientation weighting factors are thus believed to be real and indicate a change in the relative proportions of the types of dislocations in the alpha phase as a function of temperature.

The peak overlap that occurs due to the formation of the α' and α" phases (Fig. 7) also has an effect on the measured α-phase pole figures (Fig. 4). Of the five pole figures measured, only the $(10\bar{1}2)$ pole figure does not contain a contribution from the α" phase. All of the other pole figures contain a superposition of the textures of the α, α', and α" phases. As a result, the measured pole figures are affected to a degree dependent on the volume fraction and specific texture of the phases that are formed.

4.3 Beta-phase dislocation densities

Fourier analysis of the shape of the diffraction line for $(110)_\beta$ for the RD specimens was performed in order to estimate M in the beta phase. This diffraction peak and specimen orientation were selected because of the low volume fraction of retained beta and thus the need to rely on the strongest peak possible (Fig. 9). In all cases, M was estimated to be in the range of one (Table 1), thus indicating that the dislocations in the beta phase were also homogeneous and quasi-regularly distributed [22].

In light of the measured texture (Fig. 9) and low volume fraction of retained beta, it was not possible to select a quasi-random peak for the dislocation-density analysis. Instead, the FWHM of the (110), (200), and (220) beta-phase peaks from the ND, TD, and RD specimens were averaged to try to minimize the effect of texture on the calculation. The composite FWHMs of the individual peaks were then employed to obtain a modified Williams-Hall plot, whose slope was used to estimate the dislocation density in the retained beta phase.

The dislocation density of the beta-phase was found to *increase* nonlinearly in the temperature range from 800°C to 925°C (Fig. 10). This increase can be attributed to several factors acting singly or in combination: (1) changes in the effective coherent-scattering domain size of the beta phase (analogous to grain size effects in equiaxed materials), (2) changes in the strain accommodated by the beta phase (Fig. 6), (3) dislocations produced in the retained beta phase during water quenching following rolling, and (4) the formation of orthorhombic α" phase.

Because the possible influence on dislocation density changes on the effective coherent-scattering domain size in the beta-phase are contained in the intercept (γ/D) of the modified Williams-Hall plot, the first effect can be ruled out. With regard to the

second factor, the dislocation density in the beta-phase was also plotted in Fig. 10 as function of the strain accommodated in the beta phase (ε_β) determined from by the self-consistent strain-partitioning model described in Section 2.3. At 800°C, at which approximately 20 pct. beta phase is present, the predicted amount of strain imposed on the beta is ~ 0.19. At the higher rolling temperatures (~950°C), at which the volume fraction of the beta is approximately 70%, the strain suffered by the beta phase is reduced to ~ 0.14. If ρ is assumed to be proportional to ε_β, the dislocation density developed during rolling would be expected to *decrease* with increasing temperature, a behavior which is not observed. As such, the second effect is ruled out. With regard to the third factor (dislocations produced and retained in the beta phase *during* water quenching), it may be concluded that dislocations are formed are a result of the stresses produced during the athermal precipitation α' and α''. As the rolling temperature is increased and more of the material undergoes a phase transformation during quenching, the number of dislocations formed in the retained beta phase may be expected to increase. With respect to the fourth factor, the lattice parameters for α" are such that its (111) and (002) peaks overlap with the (110) beta-phase peak, its (030) peak overlaps with the (200) beta-phase peak, and the (140) and (014) peaks overlap with the (220) beta-phase peak to some extent. As a result, a portion of the measured broadening is due to the presence of these peaks. Thus, an increase in the measured dislocation density is to be expected as the volume fraction of orthorhombic α" phase increases.

At temperatures above 925°C, the *decrease* in dislocation density in the beta phase can be attributed to an increase in the elimination of dislocations due to dynamic recovery processes.

Because the (110) and (200) diffraction peaks used to measure the β-phase pole figures are confounded by peak overlap with the α" phase, the formation of this phase will also have an effect on the measured β-phase pole figures. Depending on the volume fraction and the texture of α", the measured pole figures will be affected as are the α-phase pole figures. However, the degree of the effect will be greater for the beta-phase pole figures because this phase is a minor constituent in Ti-6Al-4V at ambient temperatures.

5. Conclusions

An x-ray line-broadening technique was applied to try to establish the relative activity of different slip modes and the dislocation density in the alpha and beta phases during hot working of Ti-6Al-4V with a colony-alpha microstructure. The deduced orientation weighting factors suggested that prism <a> slip is considerably easier to activate in the alpha phase than basal <a> slip at hot-working temperatures. Furthermore, the formation of the α' and α" phases during water quenching following rolling confounds the measurement of the density of dislocations generated during the imposed deformation and the textures of the alpha and beta phases for processing temperatures from which beta readily decomposes during rapid cooling.

6. Acknowledgements

This work was conducted as part of the in-house research activities of the Metals Processing Group of the Air Force Research Laboratory's Materials and Manufacturing Directorate. The support and encouragement of the Laboratory management and the Air

Force Office of Scientific Research (Dr. J.S. Tiley, program manager) are gratefully acknowledged. One of the authors (MGG) was supported through Air Force Contract F33615-00-C-5212.

References

1. Kriviglaz, M. A. and Ryaboshapka, K. P., *Fiz. Metall. Metalloved.*, 1963, **15**, 18.
2. Krivoglaz, M. A., Martynenko, O. V. and Ryaboshapka, K. P., *Fiz. Metall. Metalloved.*, 1983, **55**, 5.
3. Klimanek, P. and Kuzel, R. Jr., *J. Appl. Cryst.*, 1988, **21**, 59.
4. Kuzel, R. Jr. and Klimanek, P., *J. Appl. Cryst.*, 1988, **21**, 363.
5. Kuzel, R. Jr. and Klimanek, P., *J. Appl. Cryst.*, 1989, **22**, 299.
6. Révész, A., Ungár, T., Borbély, A. and Lendvai, J., *NanoStruct. Mater.*, 1996, **7**, 779.
7. Ungár, T. and Tichy, G., *Phys. Status Solidi A*, 1999, **171**, 425.
8. Ungár, T., Mughrabi, H. and Wilkens, M., *Acta Metall.*, 2, **30**, 1861.
9. Ungár, T., Mughrabi, H., Rönnpagel, D. and Wilkens, M., *Acta Metall.*1984, **32**, 333.
10. Ungár, T. and Groma, I. *J. Appl. Cryst.*,1989, **22**, 26.
11. Wilkens, M., *Phys. Status Solidi A*, 1970, **2**, 359.
12. Ungár, T., Gubicza, J., Hanák, P. and Alexandrov, I., *Mater. Sci. Eng. A*, 2001, **A319-321**, 274.
13. Ungár, T., *Scripta Mater.*, 2004, **51**, 777.
14. Weidner, A. and Klimanek, P., *Mater. Sci. Eng. A*, 1997, **234**, 814.

15. Klimanek, P., Weidner, A., Esling, C. and Phillippe, M. J., in *Proceedings of the 11th International Conference on the Texture of Materials,* International Academic Publishers, Beijing, China, 1996, p.1443.

16. Klimanek, P., in *X-Ray and Neutron Structure Analysis in Materials Science,* Plenum Press, New York, 1989, p. 125.

17. Klimanek, P., *Mater. Sci. Forum*, 1994, **157**, 1119.

18. Máthis, K., Nyilas, K., Axt, A., Dragomir-Cernatescu, I., Ungár, T. and Lukáč, P., *Acta Mater.*, 2004, **52**, 2889.

19. Glavicic, M.G., Salem, A.A. and Semiatin, S.L., *Acta Mater.*, 2004, **52**, 647.

20. Wilkens, M., *Acta Metall.*, 1969, **17**, 1155.

21. Wilkens, M., *Krist. Tech.*, 1976, **11**, 1159.

22. Wu, E., Gray, E. Mac A. and Kisi, E. H., *J. Appl. Cryst.*, 1998, **31**, 356.

23. Wu, E., Kisi, E. H. and Gray, E. Mac A., *J. Appl. Cryst.*, 1998, **31**, 363.

24. Ungár, T. and Borbély, A., *Appl. Phys. Lett.*, 1996, **69**, 3173.

25. Semiatin, S.L., Montheillet, F., Shen, G. and Jonas, J.J., *Metall. Mater. Trans. A*, 2002, **33A**, 2719.

26. Hill, R., *J. Mech. Phys. Solids*, 1965, **13**, 213.

27. Suquet, P.M., *J. Mech. Phys. Solids*, 1993, **41**, 981.

28. Hill, R., *J. Mech. Phys. Solids*, 1967, **15**, 79.

29. Schafler, E., Zehetbauer, M. and Ungár, T., *Mater. Sci. Eng. A*, 2001, **A319-321**, 220.

30. Ledbetter, H., Ogi, H., Kai, S., Kim, S. and Hirao, M., *J. Appl. Phys.*, 2004, **95**, 4642.

31. Ungár, T., Dragomir, I., Révész, A., and Borbély, A., *J. Appl. Cryst.*, 1999, **32**, 992.

32. Courtney, T.H., in *Mechanical Behavior of Materials*, McGraw Hill, New York, 1990.

33. Montheillet, F. and Jonas, J.J., *Metall. Mater. Trans. A*, 1996, **27A**, 3346.

34. Semiatin, S.L. and Bieler, T.R., *Metall. Mater. Trans. A*, 2001, **32A**, 1787.

35. Paton, N.E., Williams, J.C. and Rauscher, G.P., in Proceedings of the Second International Conference on Titanium Science and Technology, Plenum Press, New York, 1973, p. 1049.

36. Dunst, D. and Mecking, H., *Z. Metallkunde*, 1996, **87**, 498.

37. Lebensohn, R.A. and Canova, G.R., *Acta Mater.*, 1997, **45**, 3687.

38. Suri, S., Viswanathan, G.B., Neeraj, T., Hou, D.-H. and Mills, M.J., *Acta Mater.*, 1999, **47**, 1019.

39. Savage, M.F., Tatalovich, J., Zupan, M., Hemker, K.J., and Mills, M.J., *Mater. Sci. Eng. A*, 2001, **A319**, 398.

40. Ahmed, T. and Rack, H.J., *Mater. Sci. Eng. A*, 1998, **A243**, 206.

41. Manero, J.M., Gil, F.J. and Planell, J.A., *Acta Mater.*, 2000, **48**, 3353.

42. Zeng, L. and Bieler, T.R., *Mater. Sci. Eng. A*, 2005, **A392,** 403.

Figure Captions

Fig. 1. Surfaces examined by x-ray diffraction: (a) normal direction (ND), (b) rolling direction (RD), and (c) transverse direction (TD).

Fig. 2. Backscattered-electron images of microstructures developed in Ti-6Al-4V following water quenching after rolling to a 10 pct. reduction at (a) 800°C or (b) 975°C.

Fig. 3. Temperature dependence of the fitted orientation-factor weighting parameters for the alpha-phase of Ti-6Al-4V rolled to a 10 pct. reduction.

Fig. 4. Recalculated alpha-phase pole figures for specimens rolled to 10 pct. reduction at (a) 800°C or (b) 975°C.

Fig. 5. Alpha-phase dislocation densities calculated from the breadths of the $(20\bar{2}2)_\alpha$ diffraction lines for specimens with the RD or TD directions normal to the specimen surface.

Fig. 6. Normalized strain ($\varepsilon/\varepsilon_{ov}$) accommodated by the alpha and beta phases as a function of temperature estimated from the self-consistent model.

Fig. 7. Diffraction patterns for undeformed specimens quenched from (a) 900°C or (b) 950°C.

Fig. 8. Diffraction patterns for specimens which were water quenched following rolling to a 10 pct. reduction at (a) 900°C or (b) 950°C.

Fig. 9. Recalculated beta-phase pole figures for specimens rolled to 10 pct. reduction at (a) 800°C or (b) 975°C.

Fig. 10. Beta-phase dislocation densities as a function of rolling temperature and strain in the beta phase (ε_β) as estimated from the self-consistent model.

Table 1. Dependence of the dislocation distribution parameter (M) on rolling reduction, temperature, and volume fraction of the alpha-phase (f_α)

Reduction (pct.)	Temperature (°C)	f_α (pct.)	M_α	M_β
10.3	800	78	1.32	1.12
9.8	850	67	1.37	1.14
9.9	900	54	1.85	1.04
10.2	925	43	1.37	1.00
9.8	950	32	1.06	0.98
10.6	975	19	1.14	1.05

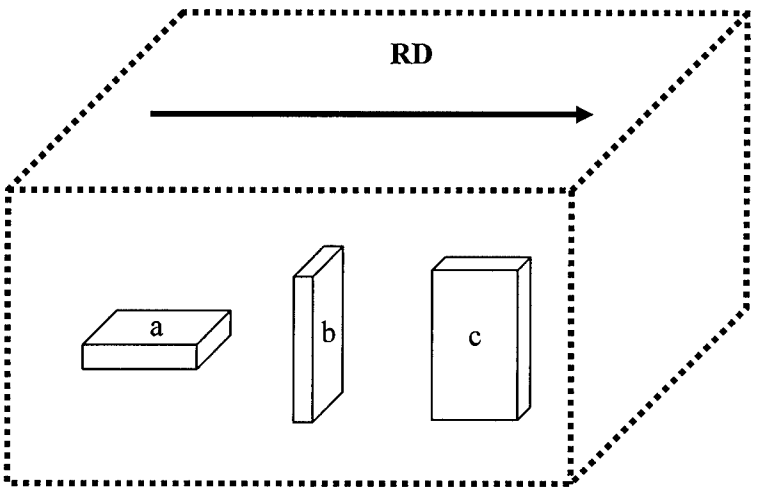

Fig. 1

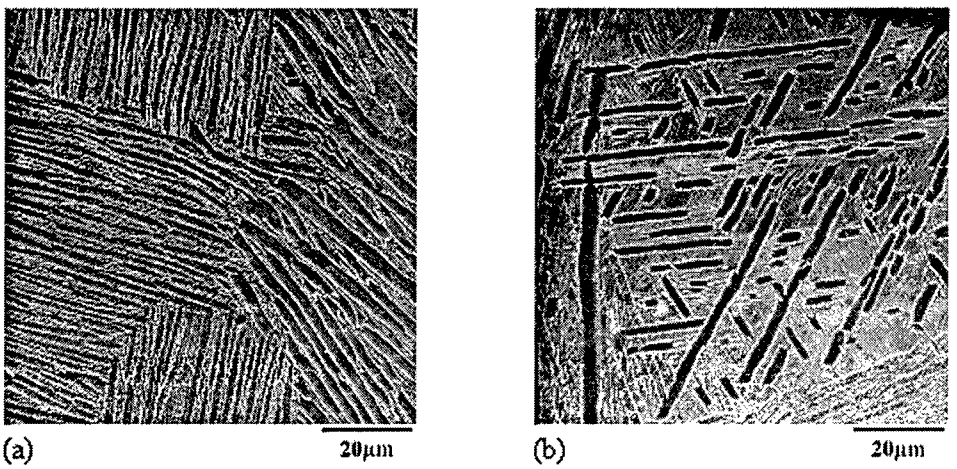

Fig. 2

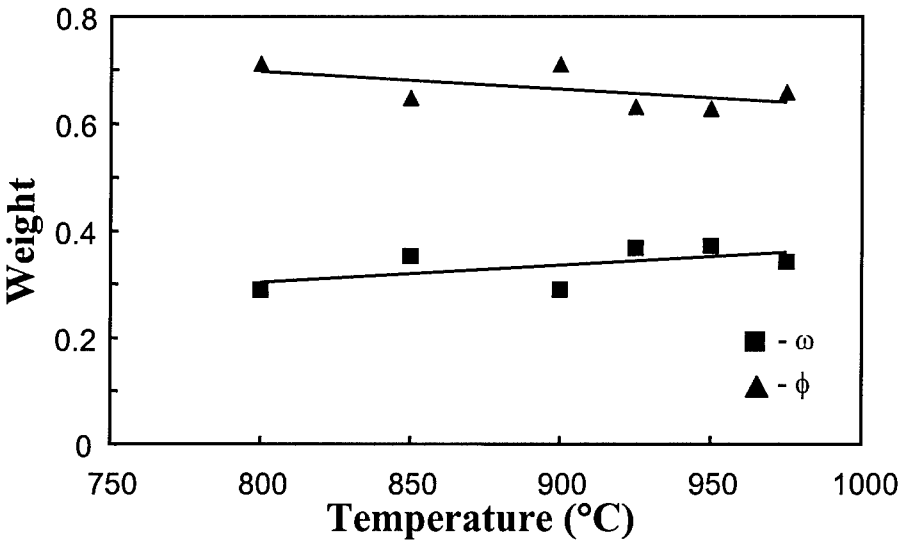

Fig. 3

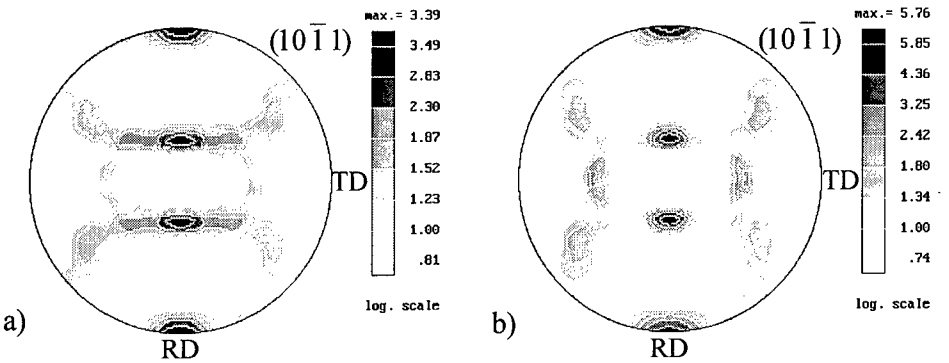
a)
(10$\bar{1}$1)
TD
RD
max.= 3.39
3.49
2.83
2.30
1.87
1.52
1.23
1.00
.81
log. scale
b)
(10$\bar{1}$1)
TD
RD
max.= 5.76
5.85
4.36
3.25
2.42
1.80
1.34
1.00
.74
log. scale

Fig. 4

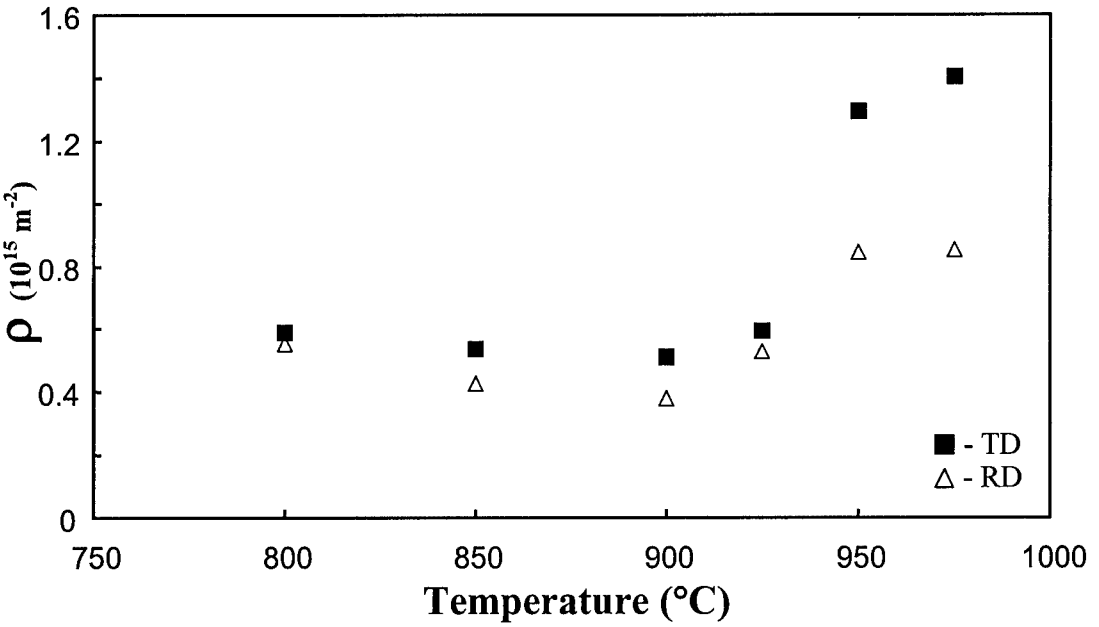
1.6
1.2
0.8
0.4
0
ρ (10^15 m^-2)
750
800
850
900
950
1000
Temperature (°C)
■ - TD
△ - RD

Fig. 5

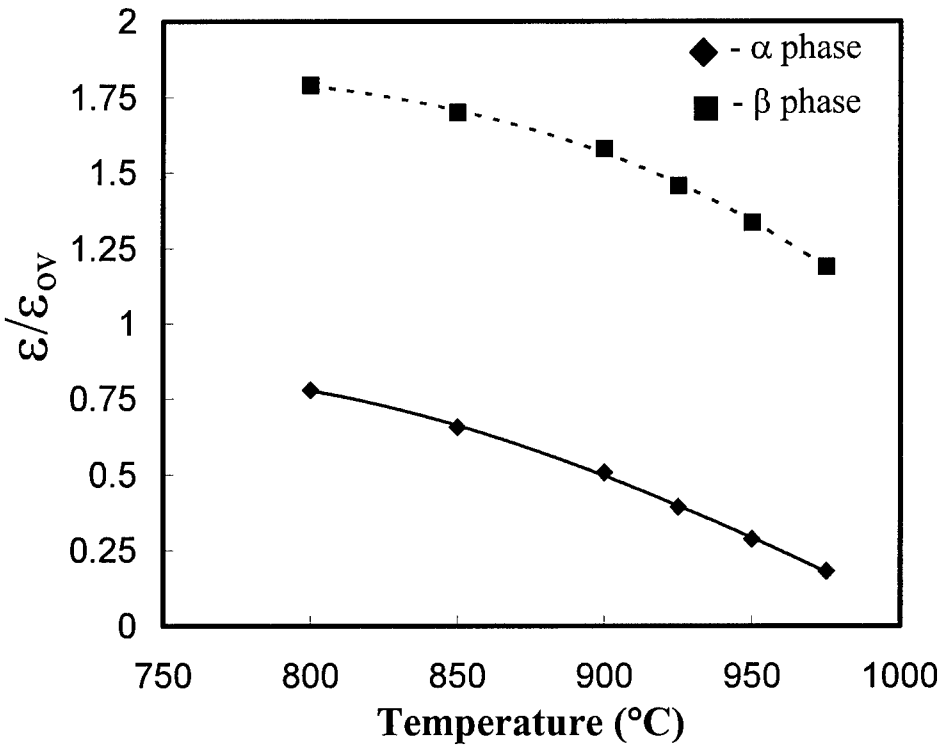
2
1.75
1.5
1.25
1
0.75
0.5
0.25
0
$\varepsilon/\varepsilon_{av}$
750
800
850
900
950
1000
Temperature (°C)
- α phase
- β phase

Fig 6

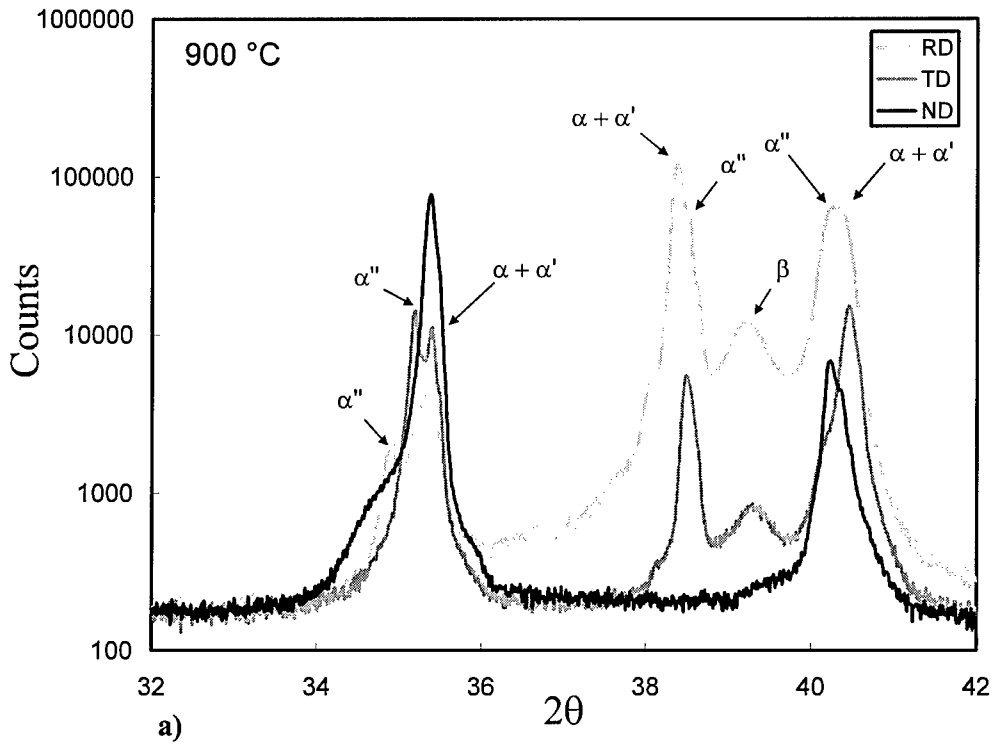
900 °C
RD
TD
ND
α + α'
α"
α"
α + α'
α"
α + α'
β
α"
1000000
100000
10000
1000
100
Counts
32
34
36
38
40
42
2θ
a)

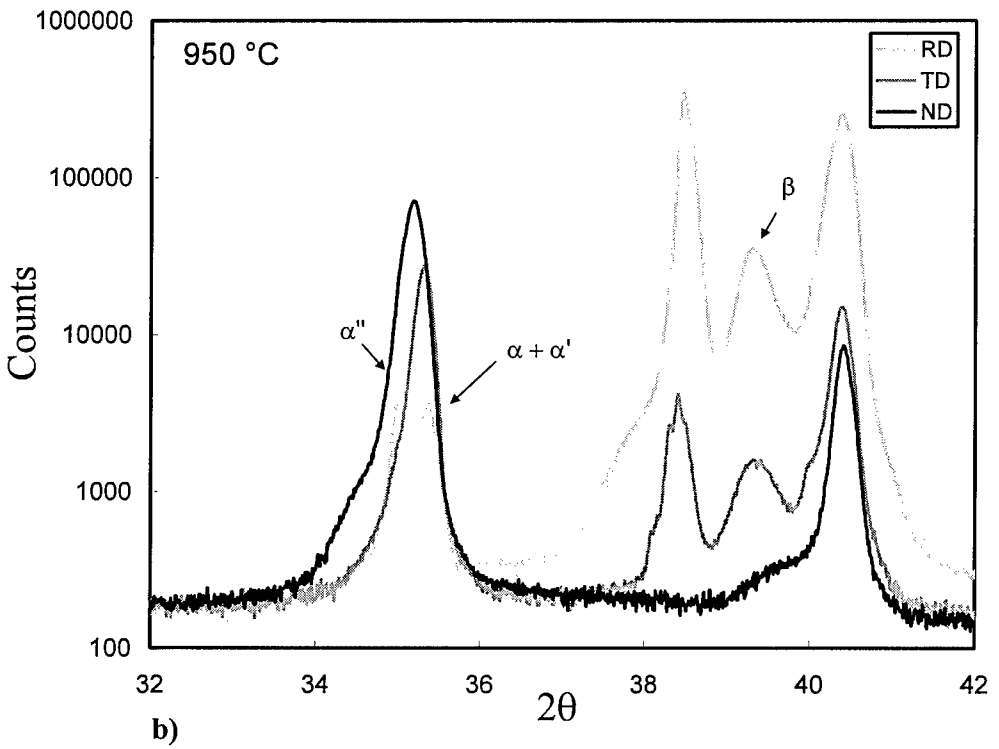
950 °C
RD
TD
ND
β
α"
α + α'
1000000
100000
10000
1000
100
Counts
32
34
36
38
40
42
2θ
b)

Fig. 7

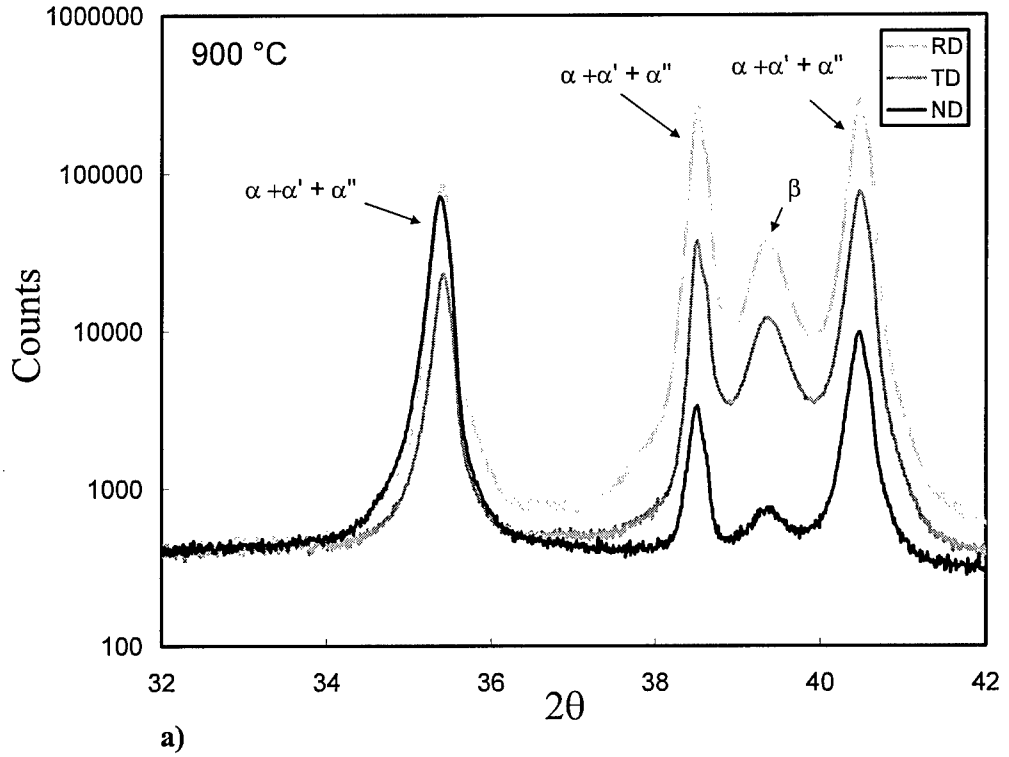
900 °C
RD
TD
ND
α +α' + α"
α +α' + α"
α +α' + α"
β
Counts
1000000
100000
10000
1000
100
32
34
36
38
40
42
2θ

a)

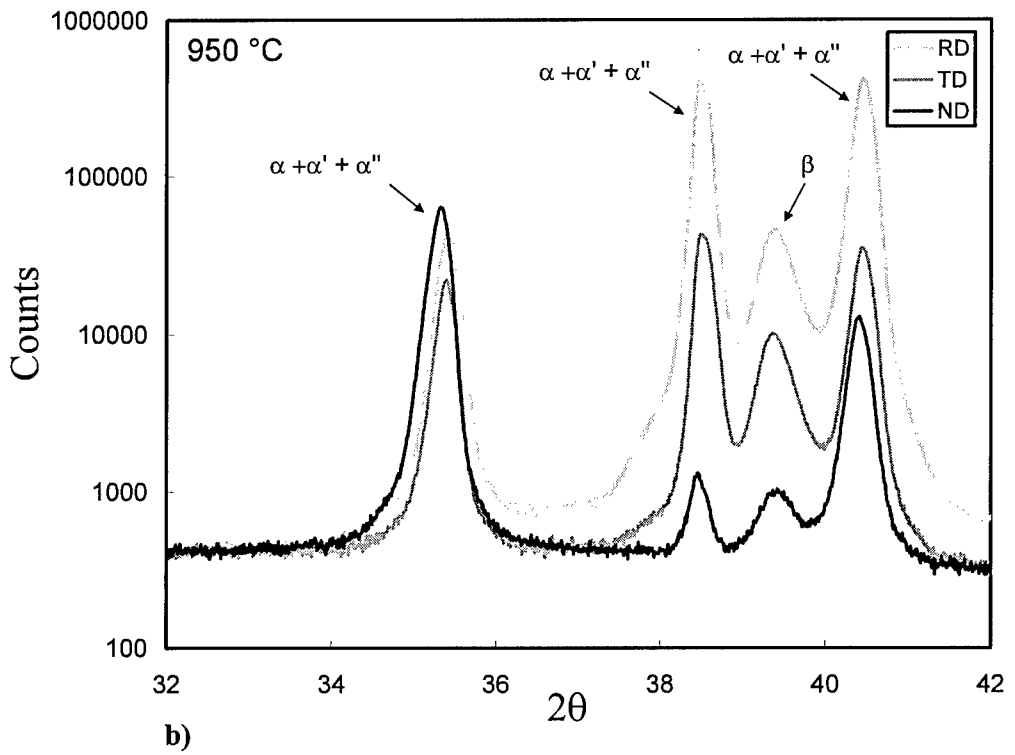
950 °C
RD
TD
ND
α +α' + α"
α +α' + α"
α +α' + α"
β
Counts
1000000
100000
10000
1000
100
32
34
36
38
40
42
2θ

b)

Fig. 8

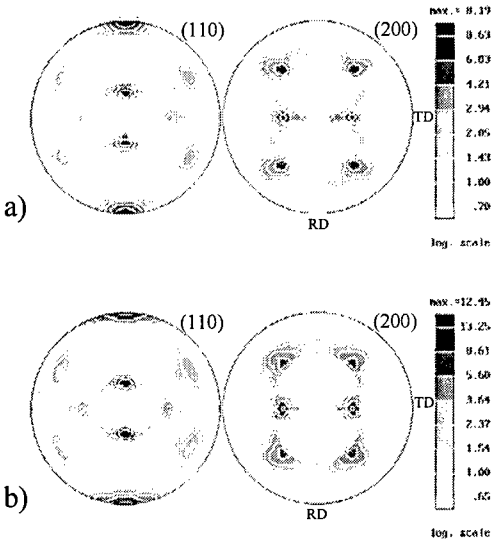

Fig. 9

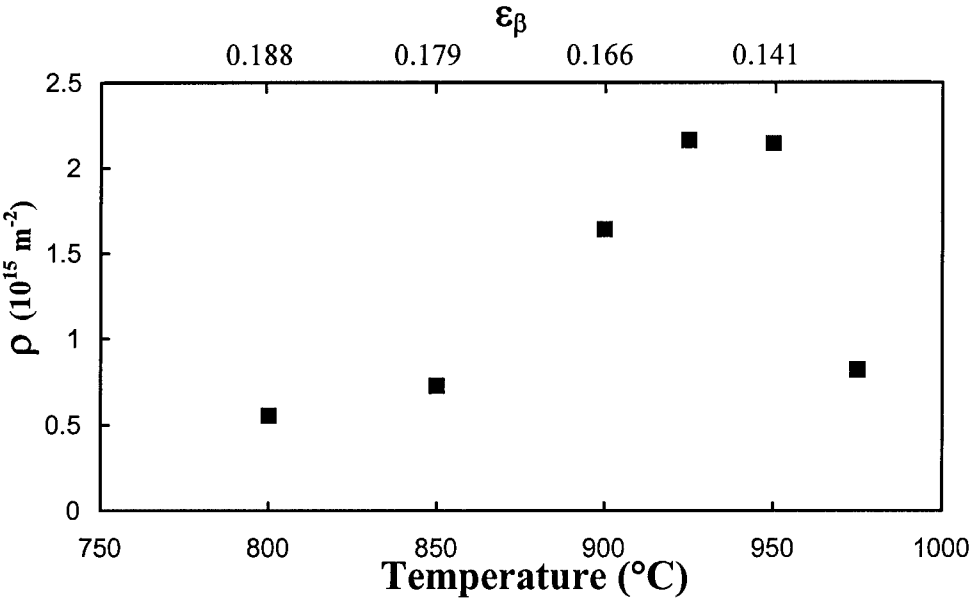
εβ
0.188
0.179
0.166
0.141
2.5
2
1.5
1
0.5
0
ρ (10^15 m^-2)
750
800
850
900
950
1000
Temperature (°C)

Fig. 10